

## Anharmonic damping in rare-gas multilayers

Burl Hall and D. L. Mills

*Department of Physics and The Institute for Surface and Interface Science, University of California, Irvine, Irvine, California 92717*

Peter Zeppenfeld, Klaus Kern, Ulrich Becher, and George Comsa

*Institut für Grenzflächenforschung und Vakuumphysik, Kernforschungsanlage Jülich, Postfach 1913, D-5170 Jülich, West Germany*

(Received 17 March 1989)

We have calculated the linewidths from anharmonic damping, for the phonon modes of rare-gas bilayers and trilayers adsorbed on the Pt(111) surface. This is done through use of perturbation theory, which in lowest order provides no damping for the monolayer vibration polarized normal to the surface. We also assume that the source of anharmonicity is the lateral interactions between adsorbates. We find linewidths in the range 0.1–0.2 meV at the temperature  $T=25$  K for all cases studied, save for the Ar bilayer, which is found to be more heavily damped. The results, supplemented by inclusion of radiative damping produced by coupling to substrate phonons, are compared with new experimental results for both the linewidth and dispersion of the normal modes of Ar, Kr, and Xe monolayers, bilayers, and trilayers adsorbed on the Pt(111) surface. The theoretical and experimental results are in good accord.

### I. INTRODUCTION

Rare-gas overlayers may physisorb on metal substrates in the form of monolayers, bilayers, and trilayers, or films consisting of a few tens of layers. Such overlayers have been studied extensively in recent years<sup>1</sup> because of their rich and subtle structural and dynamical properties. Rare gases physisorbed on graphite and metal substrate show a variety of two-dimensional (2D) phases such as the commensurate, incommensurate, and high-order commensurate phases and the corresponding phase transitions. Extensive studies of such phase transitions have shown that these systems may indeed be regarded as physical realizations of 2D systems, and therefore constitute a touchstone for the understanding of 2D matter.<sup>2,3</sup>

In addition to their structural properties, the dynamical behavior of thin rare-gas films is currently of great interest. In particular, the inelastic scattering of helium atoms may be used to probe the vibrational normal modes of these ultrathin films. Gibson *et al.*<sup>4</sup> carried out such studies for various rare-gas overlayers on the Ag(111) surface, and the dispersion curves they measure are accounted for nicely through the use of rare-gas pair potentials deduced from gas-phase data, in combination with a holding potential dependent only on the distance of the atoms above the surface plane. It has been pointed out<sup>5</sup> that even if the overlayer is adsorbed on an extremely smooth surface, as in the case of Ag(111), strong couplings between the vibrational motions in the overlayer and the substrate may still occur. The point is made best by considering a monolayer adsorbed on a substrate, regarded as perfectly smooth. If one considers the phonon normal modes of such an overlayer, with substrate atoms held fixed for the moment, one finds three branches. Two describe modes with displacement parallel to the surface,

and the third a branch polarized perpendicular to it. In the inelastic helium scattering experiments, one probes primarily the perpendicular mode.

For a monolayer, this mode is quite dispersionless, with a frequency  $\Omega_{\perp}$  independent of the wave vector  $Q_{\parallel}$  parallel to the surface. This Einstein mode has a frequency controlled by the restoring force provided by the physisorption potential well. Its frequency is in the range 2–5 meV.

Under these circumstances, there can be substantial coupling between the monolayer perpendicular mode and the substrate phonons, as discussed earlier.<sup>5</sup> For instance, if  $Q_{\parallel}$  increases from point  $\bar{\Gamma}$  in a particular direction within the surface Brillouin zone, the substrate Rayleigh wave has a frequency that increases linearly with  $Q_{\parallel}$  near  $\bar{\Gamma}$ ,  $\omega_R(Q_{\parallel})=c_R Q_{\parallel}$ . For all substrates studied, the Rayleigh wave frequency reaches values substantially larger than 5 meV at the zone boundary. Thus, the Rayleigh wave crosses and hybridizes with the perpendicular adsorbate mode. Also, near  $\bar{\Gamma}$ , the adsorbate mode lies within the bulk phonon bands of the substrate. In this frequency regime, the perpendicular adsorbate mode is damped because its energy may be radiated into the substrate in the form of bulk phonons. The mode becomes a surface resonance, with appreciable width. The hybridization of the adsorbate perpendicular mode with the Rayleigh wave, and the radiative damping just described, have been analyzed within a model which treats the substrate as a semi-infinite elastic continuum.<sup>5</sup>

Meanwhile both the wave-vector dependence of the linewidth, and the dispersion relation of phonons in krypton monolayers, bilayers, and trilayers on the Pt(111) surface, have been measured with substantially higher resolution than realized in earlier studies.<sup>6</sup> Clear evidence for the presence of the radiative damping discussed above

has been found, and the hybridization of the substrate Rayleigh wave with the adsorbate vibration has been observed. All this agrees nicely with the theoretical expectations.

The calculations reported here are motivated by aspects of these linewidth data. At large wave vectors, well beyond the radiative damping cutoff, linewidths around 0.2 meV were measured for the krypton *bilayer* and the *trilayer*, in contrast to the *monolayer* where the linewidth was too small to be resolved (less than 0.1 meV). Our calculations explore whether anharmonic interactions within the bilayer and trilayer can explain the data. We find that anharmonicity treated in the lowest order of perturbation theory provides values for the linewidth quite close to those observed. In this framework, as we shall see below, the anharmonic contribution to the linewidth of the monolayer perpendicular mode vanishes. We thus have an explanation for the origin of the substantially larger linewidths found at large wave vector for the Kr bilayers and trilayers, compared to the monolayer.

In the present calculations, we assume the dominant contribution to the anharmonic damping comes from atomic motions entirely within the adsorbed overlayers. Thus, we apply anharmonic perturbation theory to the damping of phonons confined to the overlayer itself, treating the substrate as rigid, and as the source of only the physisorption potential that provides binding for the first monolayer. For the purposes of these calculations, we have used three rare-gas pair potential functions found in the literature, and our calculated linewidths are rather insensitive to the choice of the particular potential. In addition to the krypton bilayers and trilayers explored experimentally in Ref. 6, we present the results of linewidth calculations for xenon and argon overlayers and compare them with new experimental data. The xenon linewidths are found to be comparable to the krypton case but those for the argon bilayer are much larger (0.55 meV at the  $\bar{M}$  point of the surface Brillouin zone, at the temperature  $T=25$  K).

It should be remarked that throughout this paper, we use classical lattice dynamics which begins with all atoms on a fixed lattice. We then describe the lattice motions in the harmonic approximation, and introduce anharmonicity in a perturbation-theoretic manner. We ignore quantum effects, such as the influence of a finite amplitude zero point or thermal motions on the effective force constants. In three dimensions, this approach works well for the rare-gas solids heavier than Ne. We find this picture also works well for the overlayers explored here.

## II. THE CALCULATION

We shall begin with description of the lattice dynamics of the rare-gas overlayers provided by the harmonic approximation of lattice dynamics. In this description, we include the motion of the substrate atoms by means of the approximation procedure employed in Ref. 5. When we do this, and apply the results to the krypton monolayer, we find the radiation damping rate at  $\bar{\Gamma}$  is smaller than that found experimentally by a factor of roughly 1.5. This quantitative discrepancy is not surprising in our

view, given the very simple picture of the coupling between adsorbate and substrate vibrations introduced in Ref. 5. This coupling is described by replacing the force constant  $k_0$  which has its origin in the holding potential by a renormalized force constant  $k_0(\mathbf{Q}_{\parallel}, \Omega)$  which depends on wave vector and frequency. One has<sup>5</sup>  $k_0(\mathbf{Q}_{\parallel}, \Omega) = k_0 / [1 + S(\mathbf{Q}_{\parallel}, \Omega)]$  where, as one sees from Eq. (2.16) of Ref. 5  $S(\mathbf{Q}_{\parallel}, \Omega)$  measures the amplitude of adsorbate motions in response to those in the substrate. In the present analysis of the harmonic lattice dynamics of the adsorbate substrate complex, we have multiplied  $S(\mathbf{Q}_{\parallel}, \Omega)$  in Eq. (2.16) of Ref. 5 by a factor of 2, and find this brings the theoretically calculated radiative damping rate into accord with the data.

As already mentioned, the anharmonic linewidths of the overlayer modes are calculated within a picture that assumes the only source of anharmonicity is in the interactions between rare-gas atoms in the overlayers. We calculate the linewidth of the modes assuming that the substrate atoms are held fixed in place. This linewidth is employed in the calculation of spectral density functions for the perpendicular motions of the outermost layer of adsorbate atoms by the method of Ref. 5. In this manner, an approximate description is obtained of the role of substrate atom motions in shifting the frequency of the overlayer mode. When this is done, the renormalization function  $S(\mathbf{Q}_{\parallel}, \Omega)$  is multiplied by a factor of 2 for the reason described in the previous paragraph.

If one expands the rare-gas interaction potentials in powers of the relative displacement  $\mathbf{u}(i, j) = \mathbf{u}(i) - \mathbf{u}(j)$  between atoms  $i$  and  $j$ , the lowest-order anharmonic couplings between adsorbate phonons are provided by the cubic terms. They produce damping through the interactions illustrated in Fig. 1. A phonon of interest, with frequency  $\omega_1$ , may decay by splitting into a pair of phonons, one with frequency  $\omega_2$  and one with frequency  $\omega_3$ , as shown in Fig. 1(a). In addition, the phonon of frequency  $\omega_1$  may fuse with a phonon of frequency  $\omega_2$ , to produce a phonon of frequency  $\omega_3$ . In both processes, energy is conserved, along with wave-vector components parallel to the surface, for perfectly ordered overlayers.

It is a straightforward matter to write out the cubic terms described in the preceding paragraph. Let  $\phi(|\mathbf{R}(i) - \mathbf{R}(j)|)$  be the interaction potential between atoms  $i$  and  $j$ , with  $\mathbf{R}(i)$  and  $\mathbf{R}(j)$  the instantaneous positions of the atoms. If  $\mathbf{R}^{(0)}(i)$  and  $\mathbf{R}^{(0)}(j)$  are their equilibrium positions, then we write  $|\mathbf{R}(i) - \mathbf{R}(j)| = |\mathbf{R}^{(0)}(i) - \mathbf{R}^{(0)}(j)| + \delta R(i, j)$ , where  $\delta R(i, j)$  is the change in their separation due to displacement. Then

$$\begin{aligned} \phi(|\mathbf{R}(i) - \mathbf{R}(j)|) &= \phi^{(0)}(i, j) + \phi'(i, j)\delta R(i, j) \\ &\quad + \frac{1}{2}\phi''(i, j)[\delta R(i, j)]^2 \\ &\quad + \frac{1}{6}\phi'''(i, j)[\delta R(i, j)]^3 + \dots, \end{aligned} \quad (2.1)$$

where  $\phi^{(0)}(i, j) = \phi(|\mathbf{R}^{(0)}(i) - \mathbf{R}^{(0)}(j)|)$ , and the primed quantities denote the various derivatives of the pair potential, evaluated at the equilibrium pair separation. If  $\hat{\mathbf{n}}(i, j)$  is a unit vector directed from atom  $i$  to atom  $j$ , then

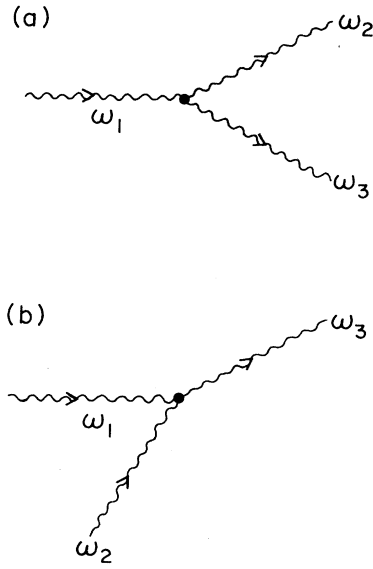


FIG. 1. A schematic illustration of the basic decay processes which emerge in the lowest order of anharmonic perturbation theory. We have (a) the two-phonon splitting process, and (b) the two-phonon difference process.

$$\begin{aligned} \delta R(i, j) = & -\hat{\mathbf{n}}(i, j) \cdot \mathbf{u}(i, j) \\ & + \frac{1}{2R_0(i, j)} \{u^2(i, j) - [\hat{\mathbf{n}}(i, j) \cdot \mathbf{u}(i, j)]^2\} \\ & + \frac{1}{2R_0^2(i, j)} [\hat{\mathbf{n}}(i, j) \cdot \mathbf{u}(i, j)] \\ & \times \{u^2(i, j) - [\hat{\mathbf{n}}(i, j) \cdot \mathbf{u}(i, j)]^2\}. \end{aligned} \quad (2.2)$$

From Eq. (2.1) and Eq. (2.2), we can collect together the various terms cubic in the displacement of the atoms. We call this term  $\phi^{(3)}(|\mathbf{r}(i) - \mathbf{R}(j)|)$ , and one finds

$$\begin{aligned} \phi^{(3)}(|\mathbf{R}(i) - \mathbf{R}(j)|) \\ = A(i, j)[\hat{\mathbf{n}}(i, j) \cdot \mathbf{u}(i, j)]^3 \\ + B(i, j)[\hat{\mathbf{n}}(i, j) \cdot \mathbf{u}(i, j)]u^2(i, j), \end{aligned} \quad (2.3)$$

where

$$\begin{aligned} A(i, j) = & -\frac{1}{6}\phi'''(i, j) + \frac{1}{2R_0(i, j)}\phi''(i, j) \\ & - \frac{1}{2R_0^2(i, j)}\phi'(i, j) \end{aligned} \quad (2.4a)$$

and

$$B(i, j) = -\frac{1}{2R_0(i, j)}\phi''(i, j) + \frac{1}{2R_0^2(i, j)}\phi'(i, j). \quad (2.4b)$$

We generate a term cubic in the atomic displacements in the vibrational Hamiltonian of the overlayers by summing Eq. (2.3) over all pairs of atoms in the monolayer, bilayer, and trilayer. The derivatives of the pair potential which appear in  $A(i, j)$  and  $B(i, j)$  are calculated from model potentials found in the literature, as described below.

To proceed, we need a more explicit notation. The lattice site of a given atom will be labeled by  $(l_{\parallel}, l_z)$ , and the equilibrium position of this atom is  $\mathbf{R}^{(0)}(l_{\parallel}, l_z)$ , and  $\mathbf{u}(l_{\parallel}, l_z)$  is its displacement from equilibrium. The phonon normal modes of the adsorbed layers, with substrate atoms held fixed, are generated by a harmonic calculation such as that described in Ref. 2. The modes are labeled by their wave vector  $\mathbf{Q}_{\parallel}$ , which lies within the appropriate surface Brillouin zone, and a second label  $\alpha$  which enumerates the various modes associated with  $\mathbf{Q}_{\parallel}$ . An  $N$ -layer structure with one atom per unit cell in each layer will have  $3N$  modes associated with each wave vector  $\mathbf{Q}_{\parallel}$ . We also have an eigenvector  $\mathbf{e}(\mathbf{Q}_{\parallel}, \alpha; l_z)$  associated with each normal mode, normalized so that

$$\sum_{l_z} \sum_{i=x,y,z} |\mathbf{e}_i(\mathbf{Q}_{\parallel}, \alpha; l_z)|^2 = 1. \quad (2.5)$$

The displacement  $\mathbf{u}(l_{\parallel}, l_z)$  is then written in terms of the annihilation and creation operators  $a(\mathbf{Q}_{\parallel}, \alpha)$  and  $a^\dagger(\mathbf{Q}_{\parallel}, \alpha)$  of the phonon modes of the structure:

$$\begin{aligned} \mathbf{u}(l_{\parallel}, l_z) = & \sum_{\mathbf{Q}_{\parallel}, \alpha} \left[ \frac{\hbar}{2N_s M \omega(\mathbf{Q}_{\parallel}, \alpha)} \right]^{1/2} \mathbf{e}(\mathbf{Q}_{\parallel}, \alpha; l_z) \\ & \times e^{i\mathbf{Q}_{\parallel} \cdot \mathbf{R}^{(0)}(l_{\parallel}, l_z)} \\ & \times [a(\mathbf{Q}_{\parallel}, \alpha) + a^\dagger(-\mathbf{Q}_{\parallel}, \alpha)], \end{aligned} \quad (2.6)$$

where  $\omega(\mathbf{Q}_{\parallel}, \alpha)$  is the frequency of the mode  $(\mathbf{Q}_{\parallel}, \alpha)$ . We apply periodic boundary conditions in the two directions parallel to the surface. Then  $N_s$  is the number of atoms in one plane parallel to the surface.

The cubic term in the vibrational Hamiltonian then may be written, when all terms are collected together, in the form

$$\begin{aligned} V_3 = & \frac{1}{(N_s)^{1/2}} \sum_{\mathbf{G}_{\parallel}} \sum_{\{\mathbf{Q}_{\parallel}^{(i)}, \alpha_i\}} \delta_{\mathbf{G}_{\parallel}, \mathbf{Q}_{\parallel}^{(1)} + \mathbf{Q}_{\parallel}^{(2)} + \mathbf{Q}_{\parallel}^{(3)}} M(\mathbf{Q}_{\parallel}^{(1)}, \alpha_1; \mathbf{Q}_{\parallel}^{(2)}, \alpha_2; \mathbf{Q}_{\parallel}^{(3)}, \alpha_3) \\ & \times [a(\mathbf{Q}_{\parallel}^{(1)}, \alpha_1) + a^\dagger(-\mathbf{Q}_{\parallel}^{(1)}, \alpha_1)] [a(\mathbf{Q}_{\parallel}^{(2)}, \alpha_2) + a^\dagger(-\mathbf{Q}_{\parallel}^{(2)}, \alpha_2)] [a(\mathbf{Q}_{\parallel}^{(3)}, \alpha_3) + a^\dagger(-\mathbf{Q}_{\parallel}^{(3)}, \alpha_3)], \end{aligned} \quad (2.7)$$

where the matrix element  $M$  is straightforwardly constructed from the discussion given above. Its form is complex, and will not be quoted here. In Eq. (2.7),  $\mathbf{G}_{\parallel}$  is a surface reciprocal-lattice vector, and  $\delta_{\mathbf{Q}_{\parallel}^{(1)}, \mathbf{Q}_{\parallel}^{(2)}}$  equals unity when  $\mathbf{Q}_{\parallel}^{(1)} = \mathbf{Q}_{\parallel}^{(2)}$  and vanishes otherwise.

In our calculations, we have supplemented Eq. (2.7) with the contribution from the anharmonicity of the holding potential. Our numerical calculations indicate its contribution is very small, however. Its inclusion changes the numerical value of the anharmonic linewidth by only one or two percent.

Quite clearly, Eq. (2.7) contains a description of the processes illustrated in Fig. 1. It is a straightforward golden-rule calculation to calculate the contribution to the relaxation rate of each mode from the process illustrated. The process in Fig. 1(a) is referred to as the two-phonon splitting process, and that in Fig. 1(b) the two-phonon difference process, as remarked above.

The relaxation rate of the mode  $(\mathbf{Q}_{\parallel}, \alpha)$  from the difference process is found to be, after some algebraic manipulations,

$$\Gamma^{(\text{diff})}(\mathbf{Q}_{\parallel}, \alpha) = \frac{18 A_c}{\pi \hbar^2} \int_{\text{BZ}} d^2 Q'_{\parallel} \sum_{\alpha', \alpha''} |M(\mathbf{Q}_{\parallel}, \alpha; \mathbf{Q}'_{\parallel}, \alpha'; -\mathbf{Q}''_{\parallel}, \alpha'')|^2 [\bar{n}(\mathbf{Q}'_{\parallel}, \alpha') - \bar{n}(\mathbf{Q}''_{\parallel}, \alpha'')] \times \delta(\omega(\mathbf{Q}''_{\parallel}, \alpha'') - \omega(\mathbf{Q}_{\parallel}, \alpha) - \omega(\mathbf{Q}'_{\parallel}, \alpha')) . \quad (2.8)$$

To calculate the relaxation rate of  $\mathbf{Q}_{\parallel}, \alpha$ , we begin by selecting  $\mathbf{Q}'_{\parallel}, \alpha'$ . Then if  $\mathbf{Q}_{\parallel} + \mathbf{Q}'_{\parallel}$  lies within the surface Brillouin zone, we make the assignment  $\mathbf{Q}''_{\parallel} = \mathbf{Q}_{\parallel} + \mathbf{Q}'_{\parallel}$ . If  $\mathbf{Q}_{\parallel} + \mathbf{Q}'_{\parallel}$  lies outside the surface Brillouin zone, we locate the (unique) reciprocal-lattice vector  $\mathbf{G}_{\parallel}$  that translates it back, and identify  $\mathbf{Q}''_{\parallel}$  with  $\mathbf{Q}_{\parallel} + \mathbf{Q}'_{\parallel} - \mathbf{G}_{\parallel}$ . In Eq. (2.8),  $\bar{n}(\mathbf{Q}_{\parallel}, \alpha)$  is the population of the mode  $\mathbf{Q}_{\parallel}, \alpha$  in thermal equilibrium, given by the Bose-Einstein function.

For the two-phonon splitting process, we have

$$\Gamma^{(\text{sp})}(\mathbf{Q}_{\parallel}, \alpha) = \frac{18 A_c}{\pi \hbar^2} \int_{\text{BZ}} d^2 Q'_{\parallel} \sum_{\alpha', \alpha''} |M(\mathbf{Q}_{\parallel}, \alpha; -\mathbf{Q}'_{\parallel}, \alpha'; -\mathbf{Q}''_{\parallel}, \alpha'')|^2 [1 + \bar{n}(\mathbf{Q}'_{\parallel}, \alpha') + \bar{n}(\mathbf{Q}''_{\parallel}, \alpha'')] \times \delta(\omega(\mathbf{Q}_{\parallel}, \alpha) - \omega(\mathbf{Q}'_{\parallel}, \alpha') - \omega(\mathbf{Q}''_{\parallel}, \alpha'')) , \quad (2.9)$$

where now  $\mathbf{Q}''_{\parallel} = \mathbf{Q}_{\parallel} - \mathbf{Q}'_{\parallel}$  or  $\mathbf{Q}''_{\parallel} = \mathbf{Q}_{\parallel} - \mathbf{Q}'_{\parallel} - \mathbf{G}_{\parallel}$ . The total damping rate of the adlayer phonon is the sum of that in Eq. (2.8) and Eq. (2.9):

$$\Gamma^{(\text{tot})}(\mathbf{Q}_{\parallel}, \alpha) = \Gamma^{(\text{sp})}(\mathbf{Q}_{\parallel}, \alpha) + \Gamma^{(\text{diff})}(\mathbf{Q}_{\parallel}, \alpha) . \quad (2.10)$$

The meaning of the damping rate  $\Gamma^{(\text{tot})}(\mathbf{Q}_{\parallel}, \alpha)$  is the following. Let all the phonon modes be in equilibrium, save for the mode  $(\mathbf{Q}_{\parallel}, \alpha)$  which is perturbed. If  $\bar{n}(\mathbf{Q}_{\parallel}, \alpha)$  is the equilibrium population of mode  $(\mathbf{Q}_{\parallel}, \alpha)$ , and this population is driven out of equilibrium so the number of phonons in the mode is  $n(\mathbf{Q}_{\parallel}, \alpha)$ , then Fermi's golden rule gives

$$\frac{dn(\mathbf{Q}_{\parallel}, \alpha)}{dt} = -\Gamma^{(\text{tot})}(\mathbf{Q}_{\parallel}, \alpha) [n(\mathbf{Q}_{\parallel}, \alpha) - \bar{n}(\mathbf{Q}_{\parallel}, \alpha)] . \quad (2.11)$$

That is,  $\Gamma^{(\text{tot})}(\mathbf{Q}_{\parallel}, \alpha)$  describes the rate at which the phonon population returns to equilibrium.

The inelastic helium scattering experiments of interest here do not probe the population of the mode  $(\mathbf{Q}_{\parallel}, \alpha)$ , but instead measure the Fourier transform of the equilibrium displacement-displacement correlation function  $\langle u_{\perp}(\mathbf{Q}_{\parallel}, l_z; t) u_{\perp}(\mathbf{Q}_{\parallel}, l_z; 0) \rangle$ , where  $l_z$  refers to the outermost layer of the structure. It is the perpendicular component of displacement of the atoms in the outermost layer that is probed predominantly, and we have written

$$\mathbf{u}(l_{\parallel}, l_z) = \sum_{\mathbf{Q}_{\parallel}} \mathbf{u}(\mathbf{Q}_{\parallel}, l_z) e^{i\mathbf{Q}_{\parallel} \cdot \mathbf{R}^{(0)}(l_{\parallel}, l_z)} \quad (2.12)$$

for the displacement operator in Eq. (2.6).

The displacement-displacement correlation function described in the preceding paragraph may be analyzed by diagrammatic perturbation theory. If the only source of decay of the mode amplitude is the two processes illustrated in Fig. 1, then the *full* width at half maximum of

the phonon peaks in this correlation function is given by  $\Gamma^{(\text{tot})}(\mathbf{Q}_{\parallel}, \alpha)$ . The decay time associated with the displacement amplitude is twice as long as that associated with the mode population. The calculations below report values of  $\Gamma^{(\text{tot})}(\mathbf{Q}_{\parallel}, \alpha)$ , and these should then be compared with the full width at half maximum of the loss structures observed in He scattering. (The width we calculate is not the width observed in an actual time of flight scan, notice. The quantity  $\Gamma^{(\text{tot})}$  is the width appropriate to a constant  $\mathbf{Q}_{\parallel}$  scan of the phonon structure.)

We can now see that the present calculation gives zero for the linewidth of the perpendicular vibrational mode of the monolayer. Any finite width for this mode from anharmonicity must come from higher-order processes that go beyond the present treatment. We can see this as follows.

In the harmonic approximation, we have three modes for each  $\mathbf{Q}_{\parallel}$ , for the monolayer. One has displacement strictly normal to the surface, as discussed earlier. The remaining two are parallel modes. If  $\mathbf{Q}_{\parallel}$  is directed along a high-symmetry line, one mode will be a shear horizontal mode, and one a longitudinal mode. For general  $\mathbf{Q}_{\parallel}$ , the two transverse modes are mixed shear and longitudinal character.

In Fig. 1, let the mode  $\omega_1$  be the perpendicular mode. If both  $\omega_2$  and  $\omega_3$  are perpendicular modes, obviously the interaction fails to conserve energy, because all three are Einstein modes. If one of these (say,  $\omega_2$ ) is a perpendicular mode, and the other is transverse, the Einstein character of the perpendicular branch requires the frequency of the transverse wave to be zero. The phase space associated with the decay processes is thus vanishingly small, and  $\Gamma^{(\text{tot})}$  is zero.

The only possibility is then that both  $\omega_2$  and  $\omega_3$  are transverse. But then the matrix element

$M(\mathbf{Q}_{\parallel}^{(1)}, \alpha_1; \mathbf{Q}_{\parallel}^{(2)}, \alpha_2; \mathbf{Q}_{\parallel}^{(3)}, \alpha_3)$  vanishes. This is seen most easily from Eq. (2.3). The presence of the three phonons must contribute a term to  $\phi^{(3)}$  that involves the product of their displacements for the matrix element to be nonzero [see Eq. (2.3)]. That is, imagine the crystal is quiescent, and we introduce a quantum of each of the three phonons involved in the decay. Then the displacement induced in the crystal gives rise to the bond-length modulation  $\mathbf{u}(i, j) = \mathbf{u}^{(1)}(i, j) + \mathbf{u}^{(2)}(i, j) + \mathbf{u}^{(3)}(i, j)$ , where  $\mathbf{u}^{(1)}(i, j)$  comes from the perpendicular mode, and  $\mathbf{u}^{(2)}(i, j)$  and  $\mathbf{u}^{(3)}(i, j)$  come from the parallel modes. For  $M$  to be nonzero, we need a term like  $u_{\alpha}^{(1)}(i, j)u_{\beta}^{(2)}(i, j)u_{\gamma}^{(3)}(i, j)$ , where  $\alpha, \beta$ , and  $\gamma$  refer to the three Cartesian directions. For the monolayer, all the vectors  $\hat{\mathbf{n}}(i, j)$  lie within the plane. Thus, the term in Eq. (2.3) which involves  $[\hat{\mathbf{n}}(i, j) \cdot \mathbf{u}(i, j)]^3$  cannot contribute to the coupling of interest. Also, since  $\mathbf{u}^{(1)}(i, j)$  is perpendicular to  $\mathbf{u}^{(2)} + \mathbf{u}^{(3)}$ , we have

$$\begin{aligned} & [\hat{\mathbf{n}}(i, j) \cdot \mathbf{u}(i, j)] u^2(i, j) \\ &= \hat{\mathbf{n}}(i, j) \cdot [\mathbf{u}^{(2)}(i, j) + \mathbf{u}^{(3)}(i, j)] \\ & \quad \times \{ [\mathbf{u}^{(1)}(i, j)]^2 + [\mathbf{u}^{(2)}(i, j) + \mathbf{u}^{(3)}(i, j)]^2 \}. \end{aligned} \quad (2.13)$$

This term contains no terms that couple one perpendicularly polarized quantum to two transverse quanta. It can only couple two perpendicular quanta to one transverse quantum or provide interactions between three transverse quanta. Thus it follows that to lowest order in anharmonicity, we obtain no anharmonic damping for the perpendicular mode of the monolayer. Higher-order processes, presumably weaker than those examined here, will come into play.

For cases other than the monolayer, the above conclusions change. First of all, the perpendicular modes now have dispersion. This allows the possibility that three perpendicular modes can interact in an energy conserving manner. It also allows for the phase space of two perpendicular quanta and one transverse quantum to be nonzero since the frequency of the transverse phonon can now be nonzero. Finally, we will have  $\hat{\mathbf{n}}(i, j)$  with perpendicular components (connecting atoms in different layers). This makes nonzero matrix elements possible for the case of one perpendicular and two transverse phonons. When all of this is put together, we find that this theory predicts that there will be nonzero contributions to the damping for any multilayer system from the lowest order of anharmonicity. This is exactly what is observed experimentally.

We comment next on aspects of the numerical work. For each  $\mathbf{Q}_{\parallel}$ , we need a mesh of  $\mathbf{Q}'_{\parallel}$  points over which we will sum in order to evaluate the integrals of Eqs. (2.8) and (2.9). What we have done is to construct a mesh of  $\mathbf{Q}'_{\parallel}$ 's with 100 points to cover the surface Brillouin zone. We find this gives convergent results. If the real-space unit vectors are (with  $a_0$  being the nearest-neighbor distance)

$$\mathbf{a} = a_0 \hat{\mathbf{x}} \quad \text{and} \quad \mathbf{b} = a_0 \left( -\frac{1}{2} \hat{\mathbf{x}} + \frac{1}{2} \sqrt{3} \hat{\mathbf{y}} \right) \quad (2.14a)$$

then the reciprocal-space unit vectors are

$$\mathbf{A} = \frac{4\pi}{\sqrt{3}a_0} \left( \frac{1}{2} \sqrt{3} \hat{\mathbf{x}} + \frac{1}{2} \hat{\mathbf{y}} \right), \quad \mathbf{B} = \frac{4\pi}{\sqrt{3}a_0} \hat{\mathbf{y}}. \quad (2.14b)$$

We then define  $\mathbf{Q}'_{\parallel} = (m\mathbf{A} + n\mathbf{B})/10$  where  $-4 \leq m, n \leq 5$ . This gives us 100 points, but they form a parallelogram-shaped grid, so that we need to fold those points that lay outside the Brillouin zone back into it. This gives us a 100-point mesh centered on  $\bar{\Gamma}$ . To do a general point  $\mathbf{Q}_{\parallel}$ , we need to find  $\mathbf{Q}_{\parallel} + \mathbf{Q}'_{\parallel}$  and  $\mathbf{Q}_{\parallel} - \mathbf{Q}'_{\parallel}$ , fold them back into the Brillouin zone if necessary, and then find the phonon frequencies  $\omega(\mathbf{Q}_{\parallel}, \alpha)$  and phonon eigenvectors  $\mathbf{e}(\mathbf{Q}_{\parallel}, \alpha)$  for the 301 different values of these parallel wave vectors. For the next value of  $\mathbf{Q}_{\parallel}$ , we must repeat this procedure. To improve the efficiency of the calculation, we have taken advantage of the fact that the set of  $\mathbf{Q}'_{\parallel}$  form a closed set, so that the sum (or difference) of any two members is a third member. Thus if we let  $\mathbf{Q}_{\parallel}$  take only values in the set  $\mathbf{Q}'_{\parallel}$ , then  $\mathbf{Q}_{\parallel} + \mathbf{Q}'_{\parallel}$  and  $\mathbf{Q}_{\parallel} - \mathbf{Q}'_{\parallel}$  must belong to the set  $\mathbf{Q}'_{\parallel}$ . Hence, we need to calculate the phonon frequencies and eigenvectors for only the 100 values of  $\mathbf{Q}'_{\parallel}$ , and then we can calculate the anharmonic contribution to the damping for any of the values of  $\mathbf{Q}_{\parallel}$  in the set  $\mathbf{Q}'_{\parallel}$ . If we were to use the longer method to calculate the phonon frequencies for the six points in  $\{\mathbf{Q}'_{\parallel}\}$  on the  $\bar{\Gamma} - \bar{M}$  line we would need to do the eigenvalue calculation 1806 times. By using closure we reduce by a factor of 18 the number of eigenvalues and eigenvectors we need to calculate. However, we do pay a price for doing this. The longer method can calculate the damping for any point on the  $\bar{\Gamma} - \bar{M}$  and  $\bar{\Gamma} - \bar{K}$  lines. By using only  $\mathbf{Q}_{\parallel}$  which belong to the set  $\{\mathbf{Q}'_{\parallel}\}$ , we are limited to six points on the  $\bar{\Gamma} - \bar{M}$  line and four points on the  $\bar{\Gamma} - \bar{K}$  line for which we can calculate the damping.

The phonon frequencies and eigenvectors were calculated using lattice dynamics in the harmonic approximation. The overlayers were treated using the slab method, so that an  $N$ -layer system required finding the eigenvalues and eigenvectors of  $3N \times 3N$  matrix. Only central forces were used, and the dynamical matrix was constructed by summing over pair interactions numerically. This allowed us to easily vary the number of neighbors included in the dynamical matrix. Since we have used parametrized models for the rare-gas-rare-gas interactions (see the discussion below), it was easy to determine analytic forms for the first, second, and third derivatives of the pair potentials. This allowed us to calculate them for any value of the separation. Although we find the dynamical matrix to be reasonably convergent when all neighbors within  $2a_0$  of the origin were included, we summed over all neighbors within  $5a_0$  of the origin for the lattice dynamics to ensure complete convergence. We connect the substrate to all the rare-gas atoms in the layer next to it via a spring constant  $k_0$ . For a monolayer,  $k_0$  and the mass of the rare-gas atom alone control the frequency of the perpendicular mode. So  $k_0$  was chosen to match the experimentally observed frequency of the monolayer at  $\bar{\Gamma}$ . We have not included any three-body interactions such as the Axelrod-Teller interaction since our earlier work<sup>2</sup> on the rare gases on Ag(111) found them to be unimportant to the lattice dynamics on the

level which experiment can measure.

The other detail that we need to consider is the manner of treating the  $\delta$  function in the formulas. We replace it with a Lorentzian with a half-width at half maximum of 0.1 meV.

Once we have  $\Gamma^{(\text{tot})}$ , we use it as input to our previous programs<sup>5</sup> to calculate the effects of radiative damping and hybridization of the platinum Rayleigh wave with the perpendicular motion of the top layer of rare-gas atoms. This allows us to calculate the total damping from both anharmonicity in the potentials and radiation into substrate phonons, and to include the influence of hybridization on the frequencies of the modes of the structure.

There is one last technical point to be discussed before we turn to a discussion of the results, and that is the nature of the pair potentials used in the calculation. We shall assume that the lateral interactions between rare-gas atoms in the overlayers are described accurately by empirical potentials found in the literature, and deduced from gas-phase data. We ignore modifications produced by the substrate. In earlier work,<sup>4</sup> it has been established that this procedure works very well in accounting for the dispersion curves measured by helium scattering. Evidently substrate-mediated modifications in the interaction potentials are quite modest, at least for rare-gas monolayers on Ag(111), and we assume this to be the case for Pt(111) as well.

There are many empirical forms for the interaction potential of two rare-gas atoms. We have chosen to look at three of them that vary rather significantly in the number of parameters that each uses. The most complicated potential that we have used is the Barker K2 potential.<sup>7</sup> This potential is the sum of five terms, each term is a polynomial in the reduced radius  $r = R/R_m$  ( $R_m$  is the atomic separation at the minimum of the potential), and most of the terms are multiplied by exponential functions of  $r$ . The 24 parameters have been chosen to fit a wide range of physical properties from the solid-crystal to gas-phase atom-atom interactions.

The second potential is the so-called " $n(r)-6$ " potential proposed by Maitland and Smith.<sup>8</sup> It is very similar to

the Lennard-Jones potential except that the exponent of the repulsive term is a function of the atomic separation:

$$V(r) = \epsilon \left[ \left( \frac{6}{n-6} \right) \frac{1}{r^n} - \left( \frac{n}{n-6} \right) \frac{1}{r^6} \right], \quad (2.15)$$

where

$$n = 12.0 + \gamma(r-1),$$

and  $r = R/R_m$ , where  $R_m$  is the position of the minimum. It has only three parameters: the well depth  $\epsilon$ , the position of the minimum  $R_m$ , and the coefficient  $\gamma$  for the exponent.

The last potential falls in between the other two in complexity. It is the HFD-B potential proposed by Aziz and co-workers.<sup>9</sup> It has an exponential repulsive term added to an attractive potential that is the van der Waal's term plus two higher terms which all have an exponential cutoff for  $r$  less than a parameter  $D$ :

$$V(R) = \epsilon \left[ A^* e^{-(\alpha^* r + \beta^* r^2)} - F(r) \sum_{j=0}^2 C_{2j+6}^* / r^{2j+6} \right]$$

$$\text{where } F(r) = \begin{cases} 1, & r \geq D \\ e^{-(D/r-1)^2}, & r < D \end{cases} \quad (2.16)$$

The cutoff  $D$  is on the order of 1.30–1.50, so that the cutoff starts at  $R \approx 1.5R_m$ . This potential has nine parameters and they are fit by comparison of experimentally measured properties versus the same properties calculated by the potential.

In Table I, we present a comparison of the three potentials by comparing their first and second derivatives, and  $A(i, j)$  and  $B(i, j)$  for two distances  $R = 3.96$  and  $7.92 \text{ \AA}$ . These distances correspond to  $a_0$  and  $2a_0$ . It can be seen that  $\phi''$ ,  $A$ , and  $B$  at  $a_0$  vary by less than 5% between the three potentials. The values of the first derivative  $\phi'$  are about the same for the Barker and Aziz potentials but they differ up to 25% for the  $n(r)-6$  potential. The results are similar for  $2a_0$ . The important thing to notice is that the anharmonic terms fall off very strongly with increasing distance.  $A$  and  $B$  fall by about 3 orders of mag-

TABLE I. Various parameters used in the anharmonic damping calculations. In the first two columns, the units are frequency squared, with the frequency expressed in meV. The last two columns are in units of  $(\text{meV})^2/\text{\AA}$ .

Potential	$\phi'/Mr$	$r = 3.96 \text{ \AA}$		
		$\phi''/M$	$A/M$	$B/M$
$n(r)-6$	-0.166 65	12.669	-11.689	1.6207
Aziz	-0.134 27	12.391	-11.149	2.5802
Barker	-0.134 61	12.715	-11.4674	1.6224
Potential	$10^2(\phi'/Mr)$	$r = 7.92 \text{ \AA}$		
		$10^2(\phi''/M)$	$10^2(A/M)$	$10^2(B/M)$
$n(r)-6$	0.473 97	-3.4815	0.863 05	-0.249 71
Aziz	0.422 84	-3.1368	0.792 14	-0.224 73
Barker	0.404 77	-3.2151	0.853 30	-0.228 53

nitude between  $a_0$  and  $2a_0$ . This allows us to sum over only the nearest-neighbor atoms when calculating the anharmonic matrix elements. Summing over all neighbors out to  $2a_0$  changes  $\Gamma^{(\text{sp})}$  and  $\Gamma^{(\text{diff})}$  each by less than 0.75% from their values when only nearest neighbors were used. Thus, in all the results that follow, we have summed over only the nearest-neighbor atoms for the calculation of  $\Gamma^{(\text{sp})}$  and  $\Gamma^{(\text{diff})}$ .

We have also examined the effects of the anharmonicity of the substrate-rare-gas potential. We have modeled it by using the Vidali-Cole form

$$V(z) = Dg(z^*) \quad \text{where } z^* = (z - z_m)/l,$$

where  $z_m$  is the position of the minimum (and hence the position of the rare-gas monolayer). The function  $g(x)$  is defined by

$$g(x) = \frac{3}{u-3} e^{-ux/a} - \frac{1}{(x+a)^3} \quad \text{with } g(0) = -1.$$

Thus  $D$  is the depth of the potential. The spring constant  $k_0$  is then the second derivative of  $V(z)$  evaluated at  $z_m$ . Using this potential we can calculate its contribution to the anharmonic damping. We have done so for rare gases on Ag(111), and found that the substrate-rare-gas potential contributes less than 1% to the total anharmonic damping. Thus we have not included it in our calculations for Pt(111).

### III. EXPERIMENT

We have measured the phonon dispersion curves and phonon linewidths of Kr, Xe, and Ar layers physisorbed on Pt(111) using high-resolution He-atom scattering. The apparatus has been described in detail elsewhere.<sup>10</sup> We use a high-pressure He-nozzle beam which in the present measurements was liquid-nitrogen cooled and operated at a pressure of 150 bars (nozzle diameter  $5 \mu\text{m}$ ). The beam has a mean translational energy of 18.3 meV at an energy spread of 1.4% corresponding to 0.25 meV (FWHM). Time-of-flight (TOF) analysis of the scattered beam is performed using pseudorandom chopping<sup>10,11</sup> and subsequent detection in a commercial quadrupole mass analyzer. Using a channel width of  $2.5 \mu\text{s}$  at a flight path of 790 mm the resulting overall energy resolution of the TOF spectrometer is  $\sim 0.32$  meV (FWHM). The angle between the incoming and outgoing beams is fixed ( $\theta_i + \theta_f = 90^\circ$ ). The angular divergence of the incoming beam and the angle subtended by the detector are both  $0.2^\circ$ . Together with the energy spread of the incoming beam this gives an overall parallel momentum resolution of typically  $\delta q_{\parallel} \sim 0.03 \text{ \AA}^{-1}$ .

A high-quality Pt(111) surface, with a mean terrace width greater than  $2000 \text{ \AA}$  (Ref. 12) was used. Rare gases of high purity were adsorbed onto this surface by exposing the surface to a constant background pressure in the range of  $5 \times 10^{-8}$  to  $5 \times 10^{-7}$  mbar. Upon reaching the desired coverage the leak valve was turned off and the rare gas pumped away. The adsorption was carefully characterized by monitoring the specular and the diffuse elastic scattered He intensity;<sup>13</sup> the completion of the first

monolayer could be determined to within a few percent.<sup>13</sup> Multilayers were grown by additional dosing of predetermined amounts onto the completed monolayers. Using a procedure described in Ref. 14 the multilayers of all three rare gases studied (Kr, Xe, and Ar) were shown to grow in a layer-by-layer mode under the working conditions used here. Furthermore, He-atom diffraction was used to characterize the structure and orientation as well as the quality of the layers grown. All three rare gases form hexagonal overlayers on Pt(111), but while the Ar layers are aligned with the Pt(111) unit cell, Kr and Xe have their unit cells rotated by  $30^\circ$  with respect to the Pt(111) unit cell.<sup>15</sup> As shown earlier, in the case of Kr and Ar small amounts of impurities ( $< 0.2\%$ ) can drastically change the orientation from the rotated to the aligned phase for Kr (Ref. 16) and from the aligned to the rotated phase for Ar.<sup>15</sup> From the width of the diffraction peaks the mean domain size of the rare-gas layers is determined to be of the order of several hundred angstroms.

The experimental procedure and the TOF spectra for Kr layers have been reported before.<sup>6</sup> Meanwhile we have performed similar measurements for the Ar and Xe adlayers (going beyond the results presented in Ref. 14 where a lower energy resolution was used). Since all the measurements were performed along the  $\bar{\Gamma}\bar{M}$  direction of the substrate unit cell, the results for Ar are along the  $\bar{\Gamma}\bar{M}$  direction of the Ar unit cell while the Kr and Xe re-

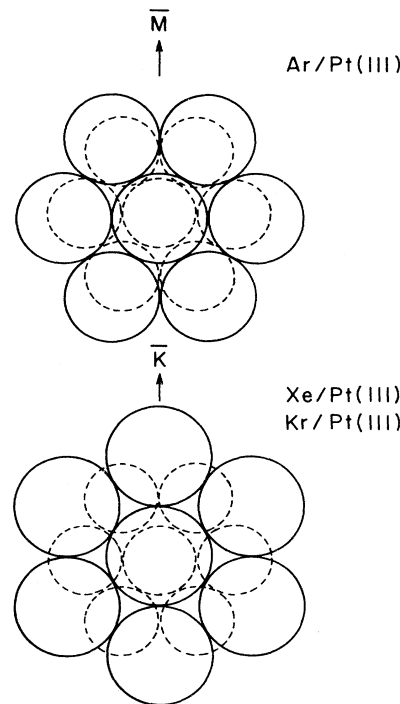


FIG. 2. The relative orientations of the Ar, Kr, and Xe with respect to the Pt(111) surface. All experimental measurements were done along the Pt(111)  $\bar{\Gamma}\bar{M}$  direction. This is the same as the  $\bar{\Gamma}\bar{M}$  direction for the Ar monolayer, but corresponds to the  $\bar{\Gamma}\bar{K}$  direction for Kr and Xe.

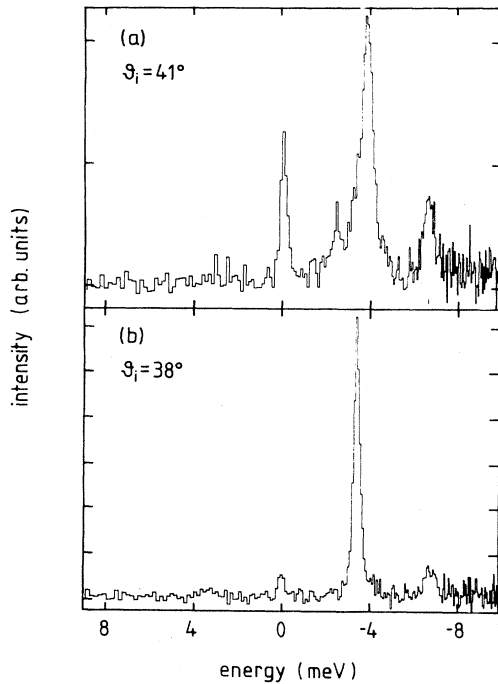


FIG. 3. Two examples of time-of-flight spectra for monolayer Xe on Pt(111) taken at the surface temperature  $T=25$  K. The main energy loss at  $-3.72$  meV (a) corresponds to momentum transfer  $q_{\parallel}=0.10 \text{ \AA}^{-1}$  near the center of the Brillouin zone, while in (b) the main energy-loss peak at  $-3.35$  meV corresponds to  $q_{\parallel}=0.57 \text{ \AA}^{-1}$  close to the zone boundary.

sults are for the  $\bar{\Gamma}\bar{K}$  direction of their own unit cells. We show the real-space lattice structure for Ar/Pt(111) and Kr,Xe/Pt(111) in Fig. 2.

As an example, Fig. 3 shows two TOF spectra of a monolayer of Xe on Pt(111) taken at a surface temperature  $T=25$  K. The scattering conditions are such that the main energy loss at  $-3.72$  meV in spectrum (a) corresponds to a parallel momentum transfer  $q_{\parallel}=0.10 \text{ \AA}^{-1}$  near the center of the Brillouin zone, while in spectrum (b) the main Xe energy-loss peak located at  $-3.35$  meV corresponds to  $q_{\parallel}=0.57 \text{ \AA}^{-1}$  close to the zone boundary. As can be seen from the figure the energy of the Xe phonon at the zone boundary is shifted by  $\sim 0.37$  meV towards lower energy as compared to the phonon energy at the zone center. Furthermore, a substantial linewidth broadening of the Xe energy-loss peak is apparent in spectrum (a) where the adsorbate mode lies within the projected bulk bands of the Pt(111) substrate. Both features can be explained by a strong vibrational coupling of the Xe adsorbate with the underlying Pt substrate, as has already been observed for Kr/Pt(111) (Ref. 6) and predicted by theory for the case of the rare gases on Ag(111) in Ref. 5. The experimental dispersion curves and in particular the behavior of the linewidth of bilayers and trilayers of Ar, Kr, and Xe on which we focus in this paper are presented below in direct connection with the results of the theoretical calculations.

#### IV. RESULTS

The first systems that we examined are the rare-gas monolayers for Pt(111).

From the calculations, which include radiative damping, we get two results. First, we get the total damping which includes anharmonic and radiative terms. Second, from the dispersion curves we obtain the difference in  $\omega_{\perp}$  between  $\bar{\Gamma}$  and the zone boundary. (See, for example, the data in Fig. 3.) As we have discussed, this mode acquires dispersion through hybridization with the Pt Rayleigh mode. Because of this, its frequency at the zone boundary is pushed down from its Einstein oscillator value. This is clearly seen in Fig. 4(a), which shows the results of a calculation for the  $\bar{\Gamma}\bar{M}$  direction of monolayer Kr/Pt(111). When we compare our calculated results using the simple model in Ref. 5 for the total damping and the frequencies of  $\omega_{\perp}$  at  $\bar{\Gamma}$  and at the zone boundary (see Table II), we find that the calculations for  $\bar{\Gamma}$  are roughly a factor of 1.5 smaller than the experimental results near the zone center for Kr and Xe. Also the frequencies of the perpendicular mode at the zone boundary are larger for all three systems than the measured values; the hybridization is not pushing down the perpendicular mode enough. As we mentioned above, according to the

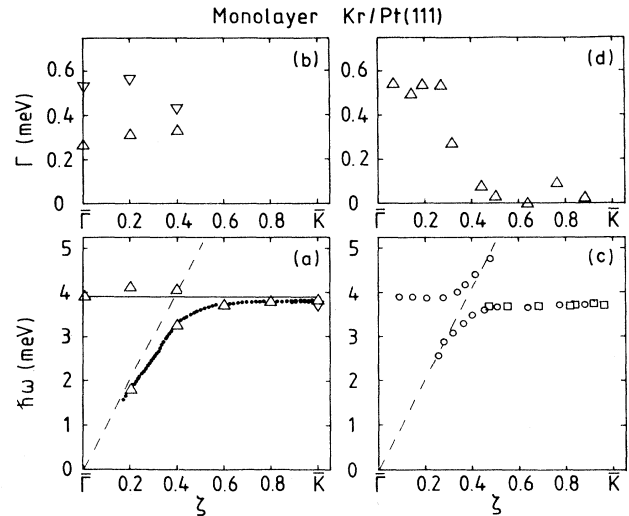


FIG. 4. For monolayer krypton on Pt(111) we compare theory for the dispersion and the linewidth of the predominantly perpendicular mode, and the data. In (a) and (b), we have theoretical results, and the data are given in (c) and (d). In (a), the solid line is the calculated dispersion, without coupling to the substrate, and the dotted line shows the dispersion with coupling to the substrate included. (b) The theoretical linewidth. As discussed in the text, only radiative damping contributes to the broadening in the monolayer. The triangles give the values produced by the treatment of Ref. 5, and the inverted triangles are values produced by doubling the function  $S$ , as discussed in Sec. IV.

TABLE II. The influence of the renormalization of the monolayer-substrate coupling constant on mode frequencies and the radiative linewidth at  $\bar{\Gamma}$ , for the various monolayers. The columns give the numbers we infer from the data and the results calculated with the coupling constant provided by Ref. 3 (column labeled  $S$ ) and those calculated with the altered coupling constant (column labeled  $2S$ ). We also give the frequencies at  $\bar{M}$  for Ar, and at  $\bar{K}$  for Kr and Xe.

	Kr monolayer									
	Expt.	Ar( $\bar{\Gamma}-\bar{M}$ )		Expt.	Kr( $\bar{\Gamma}-\bar{K}$ )		Expt.	Xe( $\bar{\Gamma}-\bar{K}$ )		
		$S$	$2S$		$S$	$2S$		$S$	$2S$	
				$\bar{\Gamma}$						
$\omega_{\perp}$ (meV)	4.85	4.84	4.84	3.90	3.90	3.88	3.70	3.70	3.67	
FWHM (meV)	0.2	0.31	0.62	0.55	0.37	0.62	0.58	0.41	0.71	
				$\bar{M}$						
$\omega_{\perp}$ (meV)	4.60	4.78	4.70	3.70	3.76	3.68	3.35	3.58	3.48	

prescription in Ref. 5, we include the effects of the substrate by renormalizing the force constant  $k_0$  to  $k_0/(1+S)$  where  $S$  is a complex number, which depends on frequency and wave vector. Its presence introduces hybridization between substrate and adsorbate motions. Frankly, we are pleased that this crude method of treating the substrate is off by only a factor of 1.5 in the estimate of the radiative damping rate. If we multiply  $S$  by a factor of 2 and recalculate we get the second set of results in Table II. This procedure improves the agreement between theory and experiment for the values of  $\omega_{\perp}$  at the zone boundary, and has also improved the agreement for the linewidth for both Kr and Xe. The agreement between the new calculation and experiment for the linewidth for Ar has worsened, although  $\omega_{\perp}$  is in much better agreement. Since the procedure of multiplying  $S$  by two results in an overall improvement, we will use it in the calculations for the bilayer and trilayer systems. As discussed earlier, the model of the adsorbate-substrate coupling employed in Ref. 3 is oversimplified, so this phenomenological procedure is reasonable. It would be interesting to see if calculations for the renormalization of  $k_0$  that treat the substrate as an fcc elastic medium would improve the basic model.

In Fig. 5, we show the results of calculations for a bilayer of Kr on Pt(111). We plot, for the four values of  $Q_{\parallel}$  in our mesh, the frequency and anharmonic linewidth found for the dominant feature in the spectral density in the  $\langle u_z u_z \rangle$  correlation function at wave vector  $Q_{\parallel}$ , for the atoms in the outermost layer. At  $\bar{\Gamma}$ , the linewidth with inclusion of radiative damping is indicated by a solid dot in Fig. 5(b). In Fig. 5(a), we show the calculated dispersion of the modes with significant perpendicular polarization as solid lines (without including the coupling to the substrate). The coarse mesh used for the linewidth calculation does not show details of hybridization with the Rayleigh wave here. The results of a more detailed calculation using the methods of Ref. 5 are shown as dots.

It should be noted that the feature which is seen experimentally depends on several modes of the rare-gas layer. Two modes are sagittally polarized, but one is perpendicularly polarized at  $\bar{\Gamma}$  while another is the longitudinal

acoustic mode at  $\bar{\Gamma}$ . These modes were referred to as  $L_1$  and  $L_2$  earlier.<sup>4</sup> Two other modes also play a role, one that is at  $\bar{\Gamma}$  the acoustic shear mode while the other is a longitudinal mode whose frequency is just below that of the lowest perpendicular mode. It is this mode that quickly acquires significant perpendicular polarization as one moves away from  $\bar{\Gamma}$ , and is the dominant perpendic-

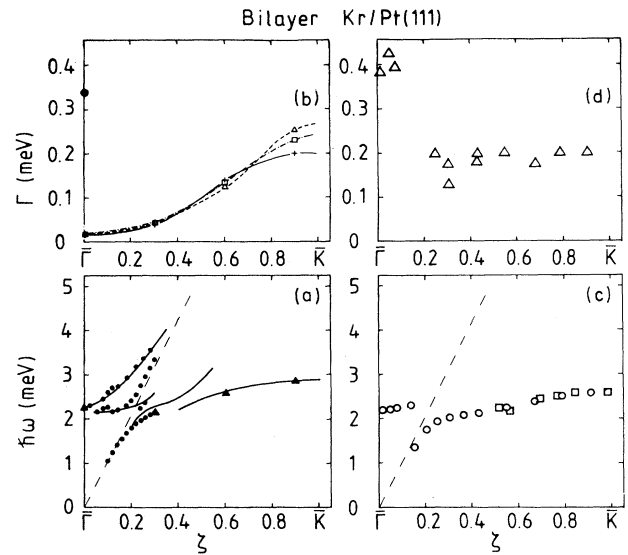


FIG. 5. The theoretical and experimental results, for the Kr bilayer on Pt(111). In (a) and (b), we have theoretical results and the data are given in (c) and (d). In (a), the solid lines are the calculated dispersions of modes with appreciable perpendicular motion in the top layer, with the substrate held rigid, and the dotted lines are the mode dispersions calculated with substrate atom motions included. The triangles show values of  $\zeta$  for which the linewidths are calculated. (b) The theoretical linewidth. The pluses and the solid line are the Barker K2 potential. The triangles and the dashed line are the Maitland-Smith  $n(r)-6$  potential, and the squares and dot-dashed line are for the Aziz potential. The large dot shows the theoretical linewidth at  $\bar{\Gamma}$ , including radiative damping.

ular mode at the point 20% of the way from  $\bar{\Gamma}$  to  $\bar{K}$  where the Pt Rayleigh mode crosses it. All the modes belong to the same symmetry class. Hence the dispersion curves of the six phonon branches cannot cross. However, in the region of an avoided crossing, two branches can exchange their polarizations. Thus the mode that is seen experimentally starts out as the frustrated perpendicular acoustic mode ( $L_1$ ). Then it changes character to the longitudinal mode ( $L_2$ ) just below  $L_1$  in frequency which carries it just out of the Pt bulk phonon bands. At that point, the mode that was the acoustic shear mode at point  $\bar{\Gamma}$  now exchanges polarization with  $L_2$  and becomes the experimentally observed mode. But it quickly loses its perpendicular polarization to the mode that was the longitudinal acoustic mode ( $L_1$ ) at point  $\bar{\Gamma}$ . For the last half of the  $\bar{\Gamma}-\bar{K}$  line this is the observed mode. The behavior of these features is thus quite complex as one scans through the zone.

The dashed line in Fig. 5(a) shows the dispersion of the platinum Rayleigh mode as calculated from its elastic constants. The Rayleigh mode couples strongly with both of the important Kr modes near  $\zeta=0.2$  where  $\zeta=Q/Q_{\max}$ . (Our convention is such that  $\zeta=1.0$  is the  $\bar{K}$  point for  $\bar{\Gamma}-\bar{K}$  and the  $\bar{M}$  point for  $\bar{\Gamma}-\bar{M}$ .) The triangles show the position of the dominant peak in the spectral density  $\rho_{zz}$  of the outermost Kr layer. It can be seen that except near the crossing of the Rayleigh mode and the perpendicular mode, the renormalization of  $k_0$  has little effect on the frequency of the perpendicular mode. Indeed, since there is now a large contribution to the components of the dynamical matrix on which the frequency of the perpendicular mode depend from the rare-gas-rare-gas potential, the effects of this renormalization are small. We will show shortly that as one might expect there is even less dependence for the trilayer systems.

In Fig. 5(b), we show the results of the calculations for the anharmonic contributions to the damping for bilayer Kr on Pt(111). The solid line shows the results for Barker's K2 potential, the dashed line for the  $n(r)$ -6 potential and the dot-dashed line for the Aziz potential. All three potentials predict the same qualitative behavior for the anharmonic contribution to the linewidth as a function of  $Q_{\parallel}$ . All three potentials predict almost the same quantitative behavior until over half way to point  $\bar{K}$  along the  $\bar{\Gamma}-\bar{K}$  line. The anharmonic contribution to the damping is small, around 0.02 meV, at  $\bar{\Gamma}$ . It then increases monotonically until the zone boundary. This behavior is controlled by the matrix element  $M(Q_{\parallel}, \alpha; Q'_{\parallel}, \alpha'; Q''_{\parallel}, \alpha'')$ .

For the perpendicular mode, it contains a factor that is the difference between the perpendicular component of displacement of a given atom, and its nearest neighbors. Thus, as  $Q_{\parallel} \rightarrow 0$  there will be no contribution from atoms in the same layer to the matrix element. At point  $\bar{\Gamma}$ , the matrix element is nonzero only by virtue of nearest neighbors in different layers. However, the perpendicular mode that is experimentally observed at point  $\bar{\Gamma}$  is the frustrated translation of the entire rare-gas crystal away from platinum crystal. Because of this, the eigenvectors for this mode have almost identical  $z$  components, even

for atoms in different layers. Thus their difference, upon which the matrix element depends, is very small. Hence the anharmonic matrix element for the perpendicular mode will be small near  $\bar{\Gamma}$ , and the linewidth is small there. From this we can deduce that almost all of the damping at point  $\bar{\Gamma}$  will be due to radiative decay into substrate phonons. Away from point  $\bar{\Gamma}$ , intralayer contributions enter, and the matrix element increases. Thus we see a rise in  $\Gamma_d$ . The dot in Fig. 5(b) shows the total damping at point  $\bar{\Gamma}$  predicted for the Kr bilayer. It shows that radiative damping accounts for over 95% of the total damping near point  $\bar{\Gamma}$ .

Comparison with the experimental data (see also Ref. 6) shows that the prediction of 0.34 meV for the linewidth at point  $\bar{\Gamma}$  is in reasonable agreement with the experimental value of about 0.38 meV. The experiments show that the linewidth falls off rather quickly near  $\zeta=0.2$ , just as the mode passes out of the Pt phonon bands. Outside the Pt phonon bands, the data give the linewidth to be relatively constant at around 0.2 meV, which is close to our calculated values. Our theory predicts that once the mode is outside the Pt phonon bands, the linewidth should be due to just the anharmonic damping. Thus, there should be a dependence on  $Q_{\parallel}$  in the linewidth, and there should be a dip in the linewidth near  $\zeta=0.3$  to a value near 0.05 meV, and then it will rise to about 0.2 meV at the zone boundary. In view of the scatter in the data, the behavior predicted by the theory cannot be ruled out.

In terms of the predicted frequencies for this perpendicular mode, we find the agreement at point  $\bar{\Gamma}$  to be within 3% of the measured value. The agreement is poorer at point  $\bar{K}$ , where the theoretical value is off by about 10%. Theory predicts a larger difference between the two frequencies than is measured experimentally. We had the same problem for the rare gases on Ag(111),<sup>4</sup> but there the disagreement was at point  $\bar{\Gamma}$ . The values given above were for the Barker K2 potential. The other two potentials give very similar results to within 1.5% of the K2 results.

In Fig. 6, we present the results of our calculations for the case of the Kr trilayer on Pt(111) together with the experimental results.<sup>6</sup> For the trilayer, the effect of the renormalization of  $k_0$  has little effect on the dispersion at the points for which we have calculated. Because the frequency of the trilayer mode is lower than that of the bilayer, the mode crosses out of the Pt phonon bands at a smaller value of  $Q_{\parallel}$ ,  $\zeta=0.16$ . This narrows the region of  $Q_{\parallel}$  for which there can be radiative damping. In Fig. 6(b) we see the predicted linewidth from anharmonic damping. It is qualitatively different from the bilayer results in that rather than being monotonically increasing, it flattens off near  $\zeta=0.6$  and stays relatively constant out to the zone boundary. The theory predicts the total damping to be 0.25 meV at point  $\bar{\Gamma}$ , and then it will be fairly constant at about 0.075 meV from  $\zeta=0.6$  to point  $\bar{M}$ . The three different potentials predict slightly different values for the linewidth from 0.072 meV for the Barker K2 to 0.082 meV for the  $n(r)$ -6 potential at  $\zeta=0.9$ . Experiment shows the linewidth to be relatively flat along

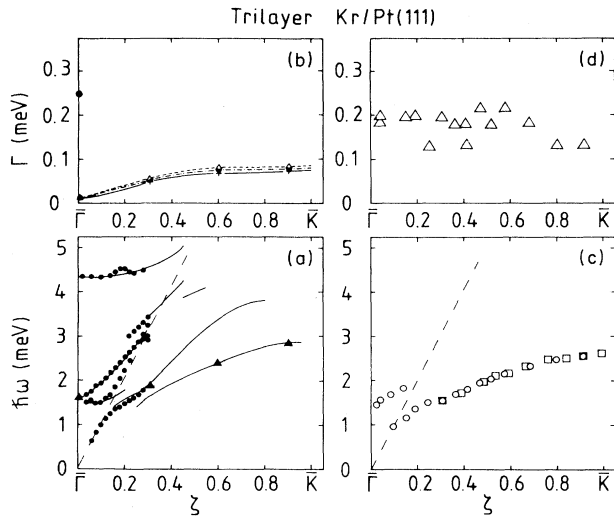


FIG. 6. The theoretical and experimental results, for the Kr trilayer on Pt(111). The conventions are the same as in Fig. 5.

the  $\bar{\Gamma}-\bar{K}$  line at about 0.2 meV. However, there are large error bars on the data, and the value of 0.07 lies with the error bars of the data.

We have concentrated our primary theoretical efforts on previously published data<sup>6</sup> on the krypton layers on Pt(111). However, we have completed calculations also for Ar/Pt(111) and Xe/Pt(111). Xenon, like krypton, has its unit cell rotated by 30° from the unit cell of the platinum. We have calculated the anharmonic damping for a bilayer of Xe/Pt(111). We found that qualitatively, its behavior is very similar to that of the bilayer of Kr on Pt(111). However, the Xe-Xe potential seems to be less anharmonic than the Kr-Kr since the calculated anharmonic damping at the zone boundary is about 0.14 meV, compared with the 0.20 meV for Kr. We do not display the Xe results in this paper.

The argon-on-Pt(111) systems are more interesting. Because the Ar monolayer frequency is much higher than the Kr or Xe monolayer frequencies, the Ar systems have more overlap in  $Q_{\parallel}$  space with the Pt phonon bands. Also the Ar overlayers have unit cells that are aligned with the Pt unit cell, as remarked earlier. This means that measurements taken along the  $\bar{\Gamma}-\bar{M}$  direction of the Pt zone will probe directions in the Ar overlayer Brillouin zones different than those probed for Xe and Kr. In Fig. 7, we show the results of calculations for an Ar bilayer on Pt(111) and the corresponding data. We can see in Fig. 7(a) that because of the higher monolayer frequency the Ar mode overlaps the Pt phonon bands out to near  $\zeta=0.3$ . (For the monolayer, they overlap out to  $\zeta=0.5$ .) Because of the larger overlap, there is a larger region where renormalization of  $k_0$  is important, with there being a 5% shift in the frequency of the mode at  $\zeta=0.4$ . We comment on the dotted lines below.

The qualitative behavior of the anharmonic contribution to the linewidth is similar to that for bilayer

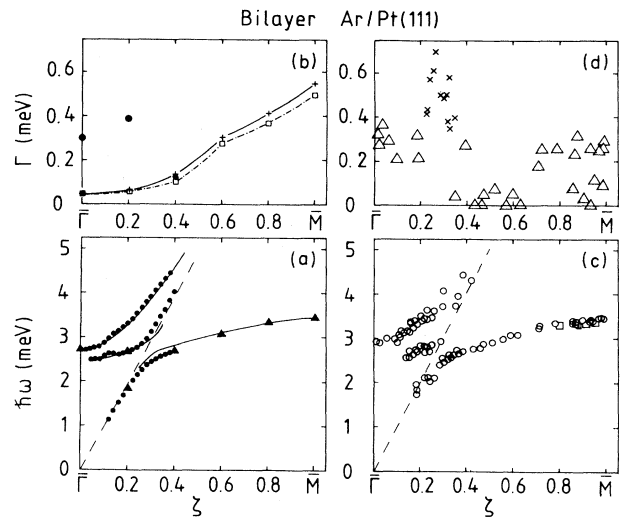


FIG. 7. The theoretical experimental results, for the Ar bilayer on Pt(111). The conventions are the same as Fig. 5. A second large dot shows the total linewidth at  $\zeta=0.2$ .

Kr/Pt(111) along the  $\bar{\Gamma}-\bar{M}$  direction, as can be seen in Fig. 7(b). It is small near point  $\bar{\Gamma}$  and then rises as one moves toward point  $\bar{M}$ . However, there is a hint of more structure in the curve. There is a slight shoulder in the curve near  $\zeta=0.6$ . There is also much stronger damping since  $\Gamma_a$  is 0.5 meV at point  $\bar{M}$  for the  $n(r)-6$  potential (it is 0.55 meV for the Barker potential). Since we can calculate for more points along the  $\bar{\Gamma}-\bar{M}$  direction for this structure with the mesh described earlier, and since there is more overlap with the bulk phonon bands for the Ar bilayer, we can calculate the radiative damping for a point other than point  $\bar{\Gamma}$ .

The total damping near the zone center is shown as the two dots in Fig. 7(b). Notice that the radiative damping has increased by 30% as we have moved away from point  $\bar{\Gamma}$  to  $\zeta=0.2$ . The anharmonic contribution to the total linewidth has hardly changed. This increase can probably be traced to the strong coupling between the Ar mode and the Pt Rayleigh wave near  $\zeta=0.2$ . This strong coupling would increase the efficiency with which the Ar mode can drive the substrate atoms, and hence would increase the rate at which it can transfer energy to the substrate. Once the mode passes out of the Pt bands, then the linewidth will drop to the anharmonic contributions. Thus the line shape is predicted to go from 0.4 meV at  $\zeta=0.2$  to 0.15 meV at  $\zeta=0.4$ . It then should increase to a value of 0.5 meV at  $\bar{M}$ .

In the new data displayed in Fig. 7(d), the dip in the linewidth just discussed is clearly present. Also, there are three distinct phonon energy-loss peaks only in a region near  $\zeta=0.2$  [Fig. 7(c)]. These three peaks are reproduced in our calculation and created by the coupling of the Pt Rayleigh mode with the  $L_1$ ,  $L_2$ , and  $\perp_1$  modes of the Ar bilayer. In the region near  $\zeta=0.2$ ,  $L_1$  and  $\perp_1$  are strongly coupled, and both of them couple strongly with the Pt Rayleigh mode. This coupling has increased the perpen-

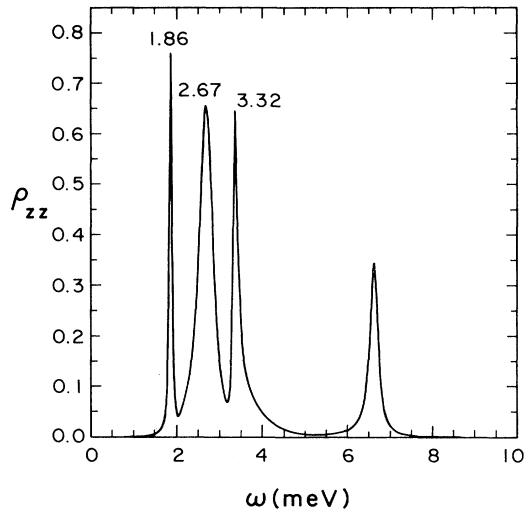


FIG. 8. The spectral density function  $\rho_{zz}(\omega)$  at  $\zeta=0.2$ , for the Ar bilayer on Pt(111). The frequencies of the three members of the dominant triplet are labeled, in units of meV.

dicular component of the  $L_1$  eigenvector. Near point  $\bar{\Gamma}$ , we have only one strong peak in the spectral density  $\rho_{zz}$ , and this is so at point  $\bar{M}$  also. As we move toward point  $\bar{\Gamma}$  from point  $\bar{M}$ , a subsidiary peak splits off, and acquires substantial oscillator strength near  $\zeta=0.2$ . We show its dispersion as a dotted line in Fig. 7(a). A high-frequency peak shows up at  $\zeta=0.2$ , so we show three modes there. The result of this mixing can be seen in Fig. 8, which shows the spectral density  $\rho_{zz}(\omega)$  of the outermost Ar layer at  $\zeta=0.2$ . The triplet structure that is the result of the mixing is very well defined, and also seen clearly in the experiment. Kr and Xe show similar behavior, but because of their lower frequencies, the peaks of the triplet lie close together, making them very difficult, if not impossible, to separate experimentally with present day resolution. For this case, we find that we get good agreement (within 3%) with the experimentally measured frequencies at  $\bar{\Gamma}$  and  $\bar{M}$ .

The results for the Ar trilayer system are presented in Fig. 9. As for the Kr trilayer, there is very little effect on the frequency of the lowest perpendicular mode from the renormalization of  $k_0$  except near the crossing point with the Rayleigh wave. The anharmonic contribution to the linewidth is small (about 0.04 meV) at point  $\bar{\Gamma}$ . It then rises until  $\zeta=0.6$  where it reaches a maximum. The anharmonic linewidth  $\Gamma_a$  has a maximum value of 0.15 meV at  $\zeta=0.6$  and falls to 0.13 meV at point  $\bar{M}$ . As usual, theory predicts that there should be a dip in the linewidth after the Ar mode leaves the Pt phonon bands. This is not in contradiction with the experiment. The behavior of  $\Gamma_a$  is not confined to the Ar trilayer. Calculations for the  $\bar{\Gamma}\bar{M}$  direction of trilayer Kr/Pt(111) show the same behavior. We do not, at this time, have a simple physical understanding of why  $\Gamma_a$  decreases after  $\zeta=0.6$ .

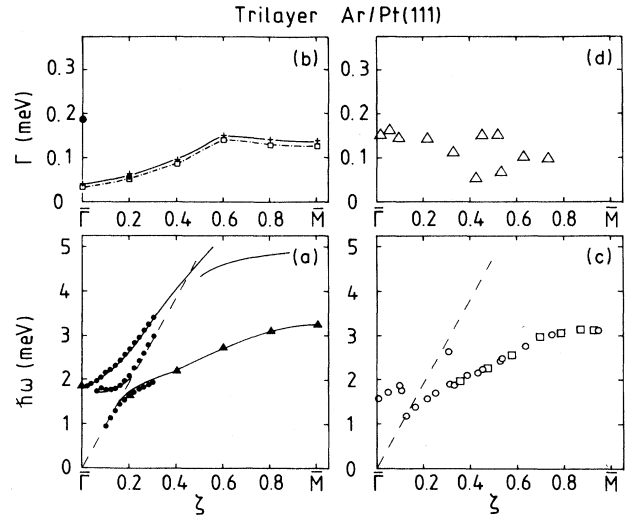


FIG. 9. The theoretical and experimental results, for the Ar trilayer on Pt(111). The conventions are the same as Fig. 5.

## V. CONCLUDING REMARKS

The experimental results presented and discussed in this paper, when set alongside the theoretical calculations, provide a rather complete description of the normal modes of rare-gas monolayers, bilayers, and trilayers on the Pt(111) surface. The use of pair potentials deduced from gas-phase data provides an adequate description of the lateral interactions between adsorbates. We see clear evidence for hybridization between the adlayer modes and the substrate phonons; recall that it is this mixing which enhances the spectral strength of the three low-frequency modes displayed in Fig. 8.

The analysis presented here elucidates two mechanisms which contribute to the damping of the overlayer modes. Near point  $\bar{\Gamma}$ , the overlayers are damped by radiation of phonons into the bulk of the material. Coupling to the substrate phonons converts the modes of the overlayer to surface resonance modes; a description of this radiative damping is contained in the harmonic approximation of lattice dynamics, as discussed earlier.<sup>5</sup> In regions of the surface Brillouin zone where the overlayer modes lie below the bulk phonon bands in frequency, in the bilayers and trilayers anharmonicity provides the dominant source of damping. Our calculations show that the data is accounted for nicely by assuming all anharmonicity resides in the lateral interactions present in the rare-gas overlayers. Once again, the use of gas-phase pair potentials provides linewidths in good accord with the data. We have carried out calculations with several choices of model pair potential, to find the results quite insensitive to the choice.

## ACKNOWLEDGMENTS

The research of two of us (B.H. and D.L.M.) is supported by the U.S. Department of Energy, through Grant No. DE-FG03-84ER45083.

- <sup>1</sup>For studies of rare-gas overlayers on Ag(111), see J. Unguris, L. W. Bruch, E. R. Moog, and M. B. Webb, *Surf. Sci.* **87**, 415 (1979); **109**, 522 (1981).
- <sup>2</sup>R. J. Birgeneau and P. M. Horn, *Science* **232**, 239 (1986).
- <sup>3</sup>K. Kern and G. Comsa, in *Chemistry and Physics of Solid Surfaces VII*, edited by R. Vanselow and R. Howe (Springer-Verlag, Heidelberg, 1988), p. 65.
- <sup>4</sup>K. D. Gibson, S. J. Sibener, Burl M. Hall, D. L. Mills, and J. E. Black, *J. Chem. Phys.* **8**, 4256 (1985).
- <sup>5</sup>Burl Hall, D. L. Mills, and J. E. Black, *Phys. Rev. B* **32**, 4932 (1985).
- <sup>6</sup>K. Kern, P. Zeppenfeld, R. David, and G. Comsa, *Phys. Rev. B* **35**, 886 (1987).
- <sup>7</sup>For Ar, the potential is given in J. A. Barker, R. A. Fisher, and R. O. Watts, *Mol. Phys.* **21**, 657 (1971), and for Xe and Kr; see J. A. Barker, M. L. Klein, and M. V. Bobetic, *IBM J. Res. Dev.* **20**, 222 (1976).
- <sup>8</sup>G. C. Maitland and G. E. B. Smith, *Chem. Phys. Lett.* **22**, 443 (1973).
- <sup>9</sup>R. A. Aziz and M. J. Slaman, *Mol. Phys.* **57**, 825 (1986) for Xe; R. A. Aziz and M. J. Slaman, *Mol. Phys.* **58**, 679 (1986) for Ar and Kr.
- <sup>10</sup>R. David, K. Kern, P. Zeppenfeld, and G. Comsa, *Rev. Sci. Instrum.* **57**, 2774 (1986).
- <sup>11</sup>L. K. Verheij and P. Zeppenfeld, *Rev. Sci. Instrum.* **58**, 2138 (1987).
- <sup>12</sup>B. Poelsema, R. L. Palmer, G. Mechttersheimer, and G. Comsa, *Surf. Sci.* **117**, 62 (1982).
- <sup>13</sup>K. Kern, R. David, R. L. Palmer, and G. Comsa, *Surf. Sci.* **175**, L669 (1986).
- <sup>14</sup>K. Kern, R. David, R. L. Palmer, and G. Comsa, *Phys. Rev. Lett.* **56**, 2823 (1986).
- <sup>15</sup>K. Kern, P. Zeppenfeld, R. David, and G. Comsa, *Vac. Sci. Technol. A* **6**, 639 (1988).
- <sup>16</sup>K. Kern, P. Zeppenfeld, R. David, and G. Comsa, *Phys. Rev. Lett.* **57**, 3187 (1986).